

Received: Received: 10 November 2018 • Accepted: 27 December 2018

Research

doi: 10.22034/JCEMA.2018.92001

Investigation into Effect of Liquefaction on Behavior of Retaining Walls

Amir Yaghouti Lighvan*, Masoud Hajjalilu Bonab

Department of Geotechnical Engineering, Faculty of Civil Engineering, Tabriz University, Tabriz, Iran

*Correspondence should be addressed to Amir Yaghouti Lighvan, Department of Geotechnical Engineering, Faculty of Civil Engineering, Tabriz University, Tabriz, Iran; Tel: +989141193200; Fax: +989141193200; Email: Amir.yaghouti@yahoo.com.

ABSTRACT

Retaining walls constructed adjacent to underground water are the structures which may be influenced by liquefaction. The design of these structures under vibration involves determining their displacements and forces caused by earthquake and liquefaction phenomena. In this study, it is attempted to assess the effect of liquefaction on the behavior of retaining walls using finite element method (FEM). The OPENSEES software is used for this purpose, which can simulate the behavior of saturated porous media using the u-P correlation formulation. Moreover, the Dafalias-Manzari critical state two-surface plasticity behavioral model is applied to simulate the behavior of sand, which can model a variety of behaviors of saturated sand in various uniaxial and cyclic loadings under drained and undrained conditions for different relative densities. The results of this study suggest that the OPENSEES software and Dafalias-Manzar behavioral model possess essential capabilities for numerical modeling of behavior of retaining walls under liquefaction conditions. The presence of retaining walls also changes the pattern of development of excess pore water pressure, particularly at middle depths of the wall.

Key words: Retaining wall, Liquefaction, Saturated sand, Critical state.

Copyright © 2018 Amir Yaghouti Lighvan et al. This is an open access paper distributed under the [Creative Commons Attribution License](https://creativecommons.org/licenses/by/4.0/).

Journal of Civil Engineering and Materials Application is published by [Raika Pajuhesh Pars](http://RaikaPajuheshPars.com); Journal p-ISSN xxxx-xxxx; Journal e-ISSN 2588-2880.

1. INTRODUCTION

Soil liquefaction is one of the most important and complicated issues in seismic geotechnics, which occurs due to undrained behavior of saturated loose sandy soils under cyclic loads and has caused widespread damage to bridges, piers, deep foundations and crucial arterial roads. The development of pore water pressure under undrained conditions is the common symptom of all liquefaction processes. When saturated loose sandy soil is exposed to rapid loading under undrained conditions, its tendency to compaction increases the pore water pressure and reduces the effective stresses. An assessment of areas with liquefied soil suggested that liquefaction often re-occurs in areas where the soil has liquefied previously and the ground conditions have not been changed yet. In other words, previously liquefied soils are prone to liquefaction in earthquakes (1). It was previously believed that the liquefaction phenomenon happens only in sandy soils. Later, it was observed that non-plastic and non-cohesive coarse-grained silt is extremely susceptible to liquefaction; liquefaction has been observed even in gravel soils under undrained conditions (1). In the San Fernando earthquake in 1906, many buildings, bridges, roads and, most important-

ly, main arterials were damaged due to liquefaction phenomenon. In this earthquake, main water supply pipes were halted in San Francisco city center due to lateral spreading, which slowed down firefighting operations in the city center after the earthquake and caused heavy casualties and financial losses in the city (2, 3). In the Alaska earthquake in 1964, the lateral spreading phenomenon devastated a great number of bridges, buildings, roads and arterials between cities such as Anchorage, Kodiak, Valdez, Sward, Portage and Whittier. In this earthquake, the lateral spreading phenomenon caused damage by approximately \$80 million and 266 bridges were destroyed entirely (4). Given the investigation into various data on lateral spreading recorded in different earthquakes, it was concluded that liquefaction-induced lateral ground movement is highly probable to occur during earthquake in the slopes terminating a canal, river or excavated area; in this case, more displacement usually occurs compared to when there is no pit or canal down the slope (4). Many coastal structures, particularly gravity quay walls, have been intensively damaged by soil liquefaction in their surroundings over the past 50 years. Hence it is so important to assess the potential of liquefaction and application of suitable techniques

for the prediction of its risks. A set of 1G shaking table tests conducted to study the deformations of a gravity quay wall under seismic loads indicated that the bed soil has a significant impact on the seismic response of a gravity wall (5). A liquefaction and lateral spreading test using a viscous fluid substituted for water demonstrated that its displacement profile patterns were extremely different from those for testing by water. These curves were very smooth with no sudden fluctuation in slope; in other words, no strain concentration was observed in the viscous fluid. However, when the shaking ended, the cumulative displacement and development of pore water pressure stopped in both tests (6-8). A quasi-plastic model used for the modeling of liquefaction suggested that liquefiable soil behaves like the flowing quasi-plastic fluid, but it loses its strength and returns to its solid behavior after the dissipation of pore water pressure and the dilation of liquefied soil. In fluid dynamics, the Reynolds' law of similarity could refer the model to the real phenomenon and relate the flow velocity to the square root of thickness of liquefiable soil layer (9). Considering the Mohr-Coulomb model for determining the development of excess pore water pressure in the sand under cyclic loading, it was found that the numerical model estimated the horizontal deformations of the wall more than actual values and predicted the vertical deformations less than measured values (10). Pile walls could mitigate structural damage in soil liquefaction conditions, resulted in a more uniform settlement in the structure (11). The studies on soil improvement against liquefaction using soil-cement walls showed that the shear probability exists along the full length of the wall in large vibrations (12). The static and dynamic studies on retaining walls with liquefiable backfills demonstrated that statics is as highly important as dynamics. The measurements on the wall and its backfill showed that the specific boundary behavior, e.g. the adsorbent materials, are less important than the soil type, input flow type and embankment length, especially when it is far larger than the height of wall (13). The effect of boundary conditions and slope on soil liquefaction indicated that variation of pore water conditions is excessive in the downstream of slope (14). An evaluation of performance of cutoff walls in reducing liquefaction-induced uplift of large underground structures showed that cutoff walls prevent the deformation of liquefied soil and high uplifts in underground structures (15). An investigation into the liquefaction-induced lateral load on a pile group behind quay wall indicated that the lateral pressure on the piles near the back of the wall is much more than that on the piles farther from the wall (16, 17). Given the importance of liquefaction phenomenon in this research, the effect of liquefaction on the behavior of retaining walls is assessed using the Dafalias-Manzari critical state two-surface plasticity behavioral model.

2. RESEARCH METHODOLOGY AND MATERIALS

The differential equations govern the general behavior of saturated porous media, which include the moment equilib-

rium equation for the whole element, the moment equilibrium equation for the fluid phase and the mass equilibrium equation. These equations are general and include dynamic and static loading and nonlinearity and geometry of materials (18). For two-phase elements, the momentum equilibrium equation for the whole element is expressed as follows (19):

$$1. \quad \text{div}\sigma + \rho b = \rho \ddot{u}_s + \rho_f \ddot{u}_{rf}$$

where σ is the total stress, u_s and u_{rf} are the displacement of solid phase and the relative displacement of fluid phase versus solid phase, respectively, ρ and ρ_f are the density for the whole element and fluid phase, respectively, and b is the body forces. The absolute displacement of fluid phase (u_f) is calculated using the equation below:

2.

$$u_f = u_s + \frac{u_{rf}}{n}$$

where n is the porosity ratio.

If the moment equilibrium equation is considered only for fluid phase, the following equation is obtained:

$$-gradP - R + \rho_f b = \rho_f (\ddot{u}_s + \frac{\ddot{u}_{rf}}{n})$$

3.

where P is the pore fluid pressure, R is the result of resistant forces caused by the fluid viscosity and $\ddot{u}_s + \frac{\ddot{u}_{rf}}{n}$ is the absolute acceleration of fluid phase. In porous media, the fluid flow is usually slow and it is possible to apply the Darcy's law as follows:

4.

$$u_{rf} = kR$$

where k is the permeability tensor which can be considered $k_{ij} = k\delta_{ij}$ in homogenous porous media. Equations 4 and 5 are combined as follows:

$$u_{rf} = k - gradP - R + \rho_f b = \rho_f (\ddot{u}_s + \frac{\ddot{u}_{rf}}{n})$$

6.

It takes a lot of time and cost to analyze the problem using the full form of equations. Depending on conditions of the problem, it is practically possible to remove some terms with slight effect on the results and simplify the problem analysis. Zienkiewicz and Shiomi (1984) claimed that the relative acceleration of fluid phase versus the acceleration of solid phase is small and negligible for moderate-frequency phenomena, e.g. earthquakes. Chan (1988) also argued that in the moment equilibrium equation of fluid

phase, the term \ddot{u}_s has a slight impact on the results and, on the other hand, causes the asymmetry of total coefficient matrix and numerical problems in the system of equations; hence it can be neglected. Neglecting the terms above, the final form of equations is thus written as follows (19).

$$\frac{\partial \sigma'_{ij}}{\partial x_j} + \frac{\partial P}{\partial x_i} + \rho b = \rho \ddot{u}_s$$

7.

8.

$$\frac{\dot{p}}{Q} + \alpha \text{div} \dot{u}_s + \text{div}\{k[-\text{grad } P + \rho_f b]\} = 0$$

Obviously, the number of equations is thus reduced from 3 to 2. These equations are abbreviated to $u - P$ formulation. In this study, this formulation is used to model the behavior of saturated porous medium. The matrix formulation of $u - P$ equations is obtained using finite element method (19):

$$9. \quad M\dot{U} + \int_V B^T \sigma' dV - QP - f^{(s)} = 0$$

10.

$$Q^T \dot{U} + HP + S\dot{P} - f^{(p)} = 0$$

where M is the mass of the system, B is the strain-displacement matrix, Q is the correlation matrix for both equations, S is the compatibility matrix and H is the permeability matrix. Vectors $f^{(s)}$ and $f^{(p)}$ include all effects of body and surface forces defined in the boundaries.

The results of Taiebat et al (2007) showed that boundary surface models are so useful to model liquefaction phenomenon and liquefaction-induced settlements (20). However, the model proposed by Dafalias and Manzari (2004) possessed more abilities than previous boundary surface models and could simulate the behavior of sand under uniform and cyclic loadings in drained and drained conditions (21). Thus, this behavioral model is used in this study to model the behavior of saturated sand. The formulation of this model is based on the boundary surface plasticity in the space relative to deviator stresses in the framework of critical state soil mechanics. In this model, the relationship between the major and minor stress ratio and the ratio of dilation stress to critical stress is determined by the state parameter. The state parameter represents the distance between the current state of soil element and the critical state line (CSL). When this parameter is used in the formulation of model, it is possible to model the behavior of a type of sand for different densities under different confining pressures using a set of constant parameters. Hence it is possi-

ble to simulate the hardening and softening behaviors, body response and development of pore water pressure in loose and dense states compared to the critical state (21, 22).

The main structure of the model is based on critical state soil mechanics. The critical state, where the deformation of specimen permanently continues under constant stresses at a volumetric strain rate of zero, happens when the stress ratio ($\eta = \frac{q}{p}$) equals the critical stress ratio (M) and the void ratio (e) equals its critical limit (e_c). The critical void ratio is just a function of effective confining pressure known as the critical state line (CSL). This equation is usually used in a logarithmic form, but its exponential form is considered in this model. According to Li and Wang (1998), the exponential equation is valid in a broader range of confining pressures (23). The equation applied for the CSL in this model is as follows (21):

$$10. \quad e_c = e_0 - \lambda_c \left(\frac{p_c}{p_{at}} \right)^\xi$$

where e_0 , λ_c and ξ are the parameters of the model and P_c and P_{at} are the confining pressure and atmospheric pressure, respectively.

In this model, the soil behavior is determined in terms of the distance from the critical state. The state parameter is used for this purpose, defined as follows (21):

$$11. \quad \psi = e - e_c$$

where e and e_c are the current and critical void ratios, respectively, defined for the same confining pressure. In the model proposed by Dafalias and Manzari (2004), this parameter is used to define the boundary stress and dilatancy stress ratios (21):

$$12. \quad M^d = M \exp(n^d \psi)$$

$$13. \quad M^b = M \exp(-n^b \psi)$$

where M , M^b and M^d are the critical stress, peak stress and dilatancy stress ratios, respectively, and n^b and n^d are the constants of the model. In this model, the dilatancy line is the same as phase change line proposed by Ishihara et al (1975) (24). A function in terms of modified Lode angle (θ) is used to generalize these equations to the three-dimensional stress space (generalization of line to surface). Figure 1 schematically shows the critical, peak and dilatancy surfaces in the surface π . When the critical, peak and dilatancy surfaces are determined, the equations of the behavioral model can be defined (21).

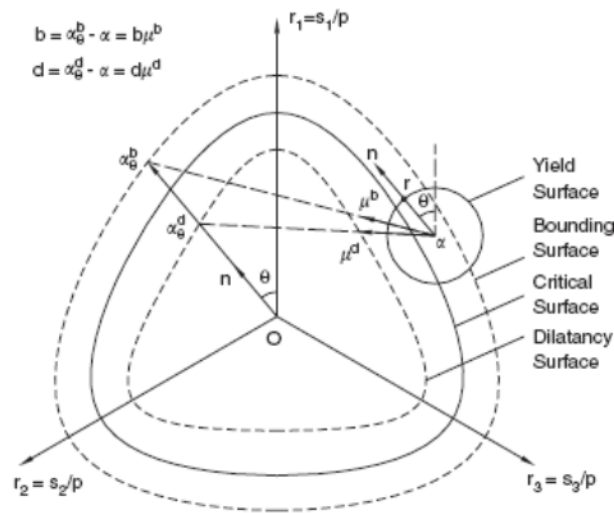


Figure 1. Schematic illustration of Manzari and Daralias model (2004) in surface π (21)

The differential equations should be integrated in the range of time to complete the numerical solution. There are a variety of methods for this purpose. These methods may be either multi-step or single-step. Two identical but independent categories are developed for single-step methods. The first category is based on residual weight and finite element in the time range, while the second category is based on the generalization of Newmark method or finite differences (25). In this study, the single-step method is utilized to solve moment equations. Given the method above, the error of moment equilibrium equation is limited to the maximum allowable error, as expressed below:

$$14. R_{t+\Delta t} = F_{t+\Delta t}^{ext} - M\ddot{U}_{t+\Delta t} - C\dot{U}_{t+\Delta t} + F(U_{t+\Delta t})^{int}$$

The values of $U_{t+\Delta t}$ and $\dot{U}_{t+\Delta t}$ are determined using the Taylor series as follows:

$$15. U_{t+\Delta t} = U_t + \Delta t \dot{U}_t + \frac{\Delta t^2}{2} \ddot{U}_t + \frac{\Delta t^3}{6} \dddot{U}_t + \dots$$

$$16. \dot{U}_{t+\Delta t} = \dot{U}_t + \Delta t \ddot{U}_t + \frac{\Delta t^2}{2} \dddot{U}_t + \dots$$

The equations are re-written by converting newton:

$$17. U_{t+\Delta t} = U_t + \Delta t \dot{U}_t + \frac{\Delta t^2}{2} \ddot{U}_t + \beta \Delta t^3 \ddot{U}_t$$

$$18. \dot{U}_{t+\Delta t} = \dot{U}_t + \Delta t \ddot{U}_t + \gamma \Delta t^2 \ddot{U}_t$$

When the equivalent finite difference of \ddot{U}_t is substituted, the final equations are expressed as below:

$$19. U_{t+\Delta t} = U_t + \Delta t \dot{U}_t + [(0.5 - \beta)\Delta t^2 \ddot{U}_t + \beta \Delta t^2 \ddot{U}_{t+\Delta t}]$$

$$20. \dot{U}_{t+\Delta t} = \dot{U}_t + [(1 - \gamma)\Delta t \ddot{U}_t + [\gamma \Delta t] \ddot{U}_{t+\Delta t}]$$

The coefficients β and γ are the parameters which control the stability and convergence of the system of equations (26). In this study, the values of β and γ are considered 0.3025 and 0.6, respectively. The time step (Δt) is one of the most important numerical parameters in time-dependent analyses. This parameter is of great importance in dynamic problems, particularly correlated problems. Given the high velocity of stress waves in solid structures, the time step of equilibrium equation must be selected as small as possible in dynamic problems for saturated porous media, so that quick changes caused by these waves are available. In this study, the time step of $\Delta t = 0.002 \text{ sec}$ is applied for the acceleration phase and time steps of 0.04 sec to 2 sec are applied for the dissipation phase of excess pore water pressure. Zienkiewicz et al studied the impact of initial stresses on soil liquefaction (19) and proposed a set of empirical equations for the calculation of K_0 in sand masses (27). Since no specific value was reported for initial stress ratios (K_0) in most tests and some researchers reached good results by the K_0 equal to 0.2, this parameter is considered 0.2 in this study (28). For the simulation of a more realistic model for the set of soil and water, the modeling should be carried out accurately and the governing equilibrium equations must be solved by correlation. Moreover, more accurate behavioral models, e.g. Dafalias-Manzari model (2004), should be utilized for more precise modeling of soil behavior. Given the requirements, the OpenSees finite element software is used for the modeling (29). In this study, the results achieved by Maharjan and Takahashi (2013) are employed to validate the numerical model. Maharjan et al prepared four specimens for centrifuge tests to investigate the impact of silt layers with lower permeability between sand layers. The tests are done on a scale of 40:1. The specimens are made in a shear box measuring 500 mm \times 200 mm \times 450 mm, which corresponds to a sand deposit 9.8 m in height on prototype scale. The Toyoura sand is used for these tests. The soil properties are listed in Table 1. The sand specimens are prepared

at relative densities of 50-55% using sand pluviation technique and there are two silt layers 1 m in height in the se-

cond specimen (on prototype scale) (30).

Table 1. Soil properties for tests by Maharjan (31)

Property	Toyoura sand
G_s	2.65
$D_{50}(mm)$	0.19
$D_{10}(mm)$	0.14
e_{max}	0.973
e_{min}	0.609
Permeability $k(m/s)$	2×10^{-4}
sand %	100%

Table 2 also presents the parameters of behavioral model used in this study.

Table 2. Parameters of Manzari's behavioral model for Toyoura sand (30)

Amount	Parameter symbol	Parameter performance
125	$G_0(kPa)$	Elastic
0.05	ν	
1.25	M	Critical state
0.712	c	
0.019	λ_c	
0.934	e_c	
0.7	ξ	
0.01	m	Yield surface
0.704	A_0	Dilatancy
3.5	n^d	
7.05	h_0	Modulus of plasticity
0.968	c_h	
1.1	n^b	
4	z_{max}	Fabric tensor
600	c_z	

In these tests, the sand layer is completely saturated and the model is rotated at an acceleration of 40g and then vibrated horizontally. The input horizontal acceleration of

this model equals the acceleration spectrum of Hachinohe Port earthquake in 1968; Figure 2 shows the acceleration on prototype scale.

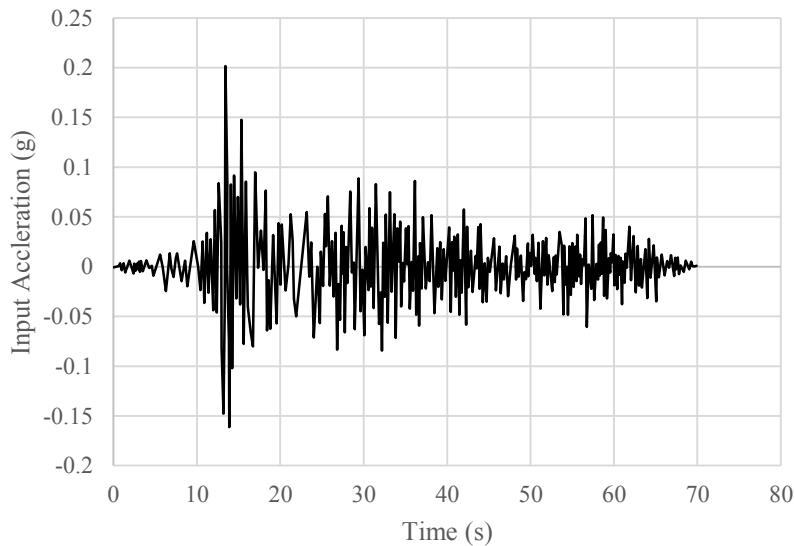


Figure 2. Acceleration spectrum of Hachinohe Port earthquake in 1968

Figure 3, Figure 4, Figure 5 and Figure 6 demonstrate the excess pore water pressures at different depths during the

vibration for the numerical and experimental models.

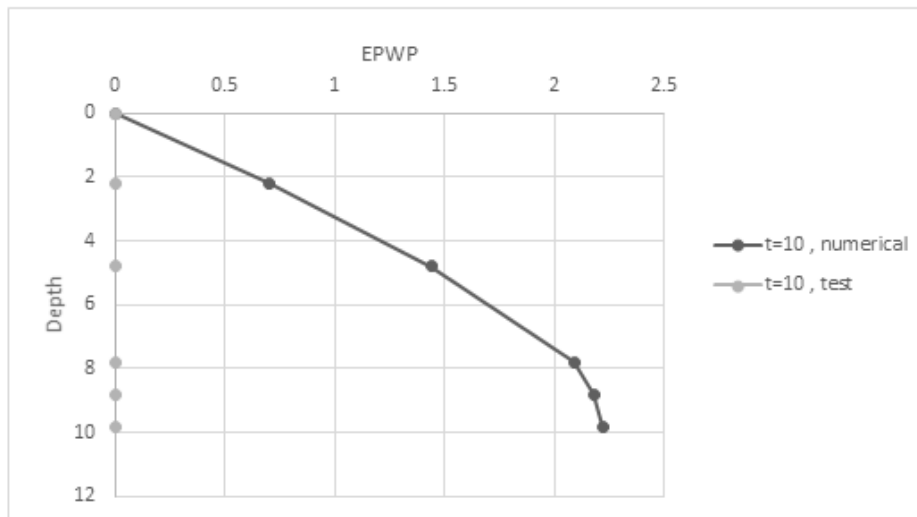


Figure 3. Excess pore water pressure at 10 sec

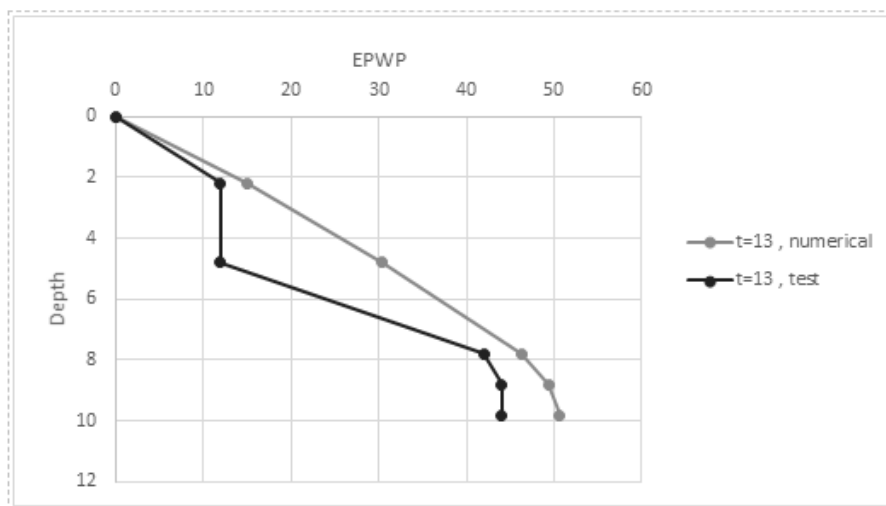


Figure 4. Excess pore water pressure at 13 sec

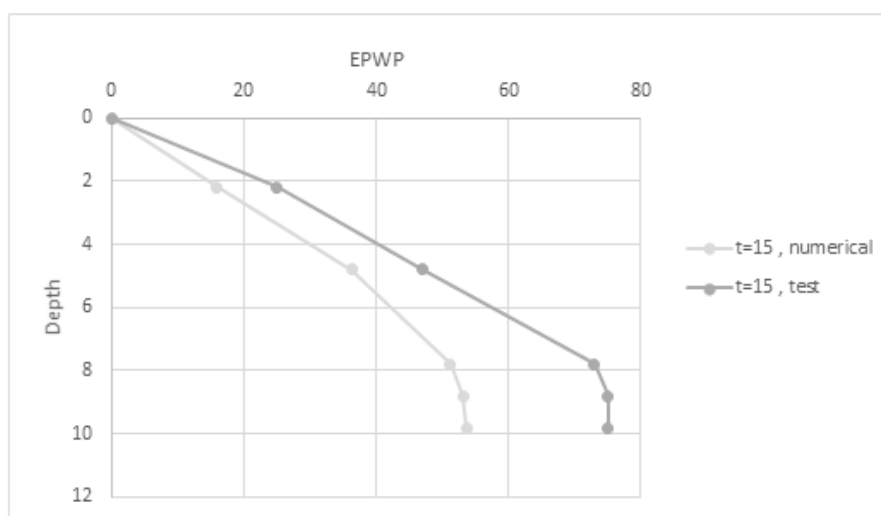


Figure 5. Excess pore water pressure at 15 sec

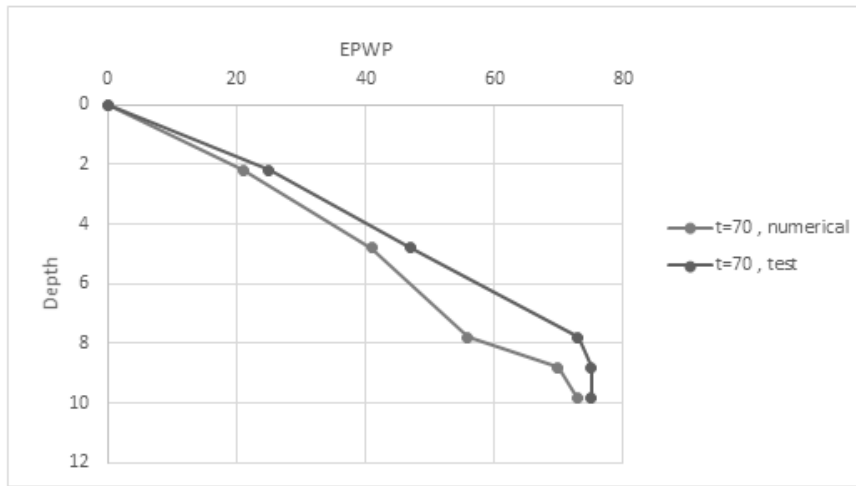


Figure 6. Excess pore water pressure at 70 sec

An investigation of the results suggests that there is good agreement between the results of excess pore water pressure at different depths for numerical and experimental

modelings. Figure 7 also shows the liquefaction-induced displacements of ground surface for numerical and experimental modelings.

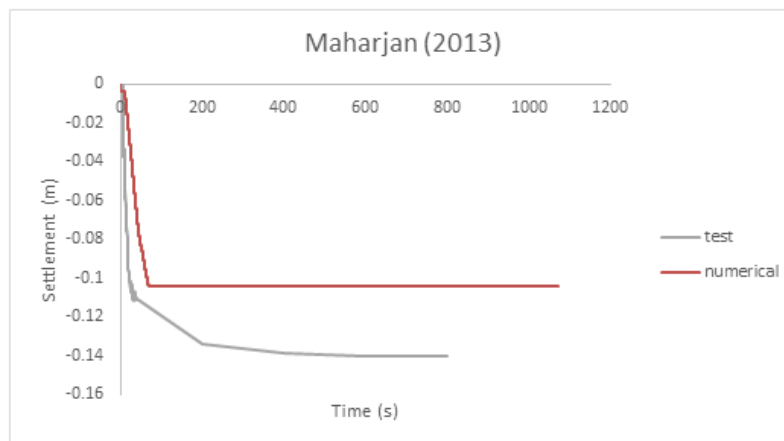


Figure 7. Ground surface settlement

This chart shows the various steps of liquefaction and the subsequent consolidation. This figure demonstrates that there is about 25% difference between the results of numerical and experimental modelings, which is acceptable because of the complexity of liquefaction phenomenon. In this study, the behavior of a gravity pier located in saturated sandy soil is examined through the numerical modeling of VELACS11 test to assess the effect of liquefaction on retaining walls (31). The VELACS11 centrifuge test is carried out at Cambridge University. This model includes an aluminum component 0.478 m long with a cross section of 0.10 m × 0.05 m, placed in the saturated sand layer as a gravity pier. In this test, a lead burden 0.002 m thick and

0.48 m wide is placed at a distance of 0.01 m on the backfill, which allows for the complete drainage of water in the backfill. This lead plate is 0.1 m in length and 0.48 m in width. The water level is 0.015 m above the surface of sand layer (31). The test box measures 0.9 m × 0.48 m × 0.22 m and its surface and bottom are rigid, inflexible and flat. In this test, the sand layer is completely saturated; the model is rotated at a centrifugal acceleration of 50g and the test box is then vibrated in its foundation horizontally. The input horizontal acceleration is approximately sinusoidal with 10 cycles of maximum amplitude of 0.25g at a frequency of 1.92 Hz on full scale. Figure 8 represents the input acceleration time history for this test (31).

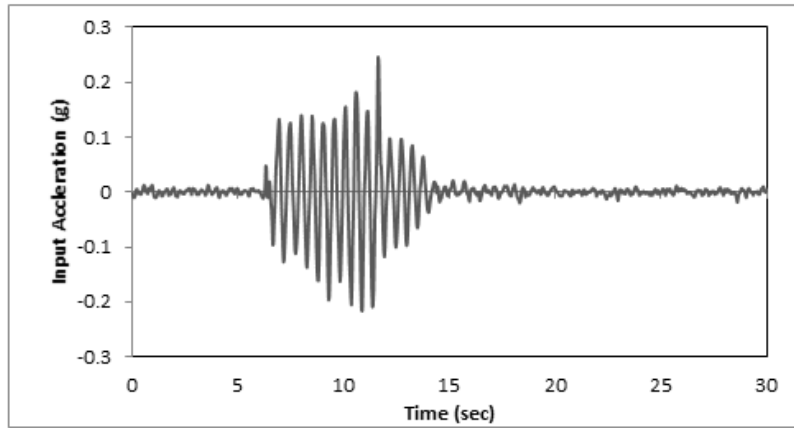


Figure 8. Input acceleration time history for VELACS11 model (31)

The Nevada sand is used at a relative density of 60% in this test. Table 3 shows the mechanical and hydraulic properties of the sand, aluminum and lead used in this test.

Table 3. Mechanical properties of Nevada sand at relative density of 60% (31)

Amount	Parameter symbol	Parameter performance
0.400	Porosity (n)	Nevada sand with D=60%
15.76	Dry unit weight (KN/m ³)	
5.6×10^{-5}	Permeability coefficient (m/s)	
2.8×10^{-3}	Permeability coefficient on full scale (m/s)	
27.16	Unit weight (KN/m ³)	Aluminum
7.0×10^7	Young modulus (KN/m ²)	
0.33	Poisson ratio	
1.0×10^{-9}	Permeability coefficient (m/s)	
110.81	Unit weight (KN/m ³)	Lead

In the modeling of this test, the Manzari-Dafalias model is used to predict the behavior of saturated sand and the aluminum wall is modeled using the elastic behavioral model. The effect of lead plate is considered along a 5 m distance from the surface of backfill under undrained condition and its rigidity is neglected. In the modeling, 4-node rectangular elements are applied for deformations and all nodes of

the element have the degree of freedom of pore water pressure. The wall nodes are connected to the backfill nodes through EDF command and the relative displacement between the soil and the wall is ignored. The parameters of Nevada sand are listed in Table 4. These parameters are calibrated.

Table 4. Parameters of behavioral model for Nevada sand (31)

Amount	Parameter symbol	Parameter performance
150	$G_0(kPa)$	Elastic
0.05	ν	
1.14	M	Critical state
0.78	c	
0.027	λ_c	
0.83	e_c	
0.45	ξ	
0.02	m	Yield surface
0.81	A_0	Dilatancy
1.05	n^d	
9.7	h_0	Modulus of plasticity
1.02	c_h	
2.56	n^b	
5	z_{max}	Fabric tensor
800	c_z	

In the modeling process, a model is initially made under static conditions. Horizontal in situ stresses are calculated by $K_0 = 0.2$. Then, each calculated in situ stress is used in the dynamic analysis as an initial stress condition. It is worth mentioning that various values of K_0 are evaluated to examine the effect of lateral in situ stresses on the behavior of retaining wall; eventually, it is found that the impact of this parameter on the wall behavior is negligible in numerical modeling. Given the analyses conducted to determine appropriate time step for obtaining the most

accurate solution and high sensitivity of this problem to the selected time step, the time step of $\Delta t = 0.002 \text{ sec}$ is employed for the calculations in this study. The selected time step has a great impact on the satisfaction of stability condition, accuracy of flow and equilibrium equations and reliability of results. It must be noted that the time step of $\Delta t = 0.002 \text{ sec}$ is firstly applied for the modeling of this test and the output values are incompatible with the test results. Therefore, it is necessary to determine the suitable time step in each modeling through sensitivity analysis or

other existing methods, so that the stability condition and accuracy of calculations are met and the calculations and analysis time are kept at a reasonable level. The differential equations are integrated within the time range to accomplish the numerical solution. Accordingly, the generation of Newmark method or finite differences is applied.

3. RESULTS, DISCUSSION AND EVALUATION

Figure 9 illustrates the liquefaction-induced permanent horizontal displacement of the wall measured by the displacement meter during the test conducted at Cambridge University and the values predicted for numerical modeling using the Manzari-Dafalias model.

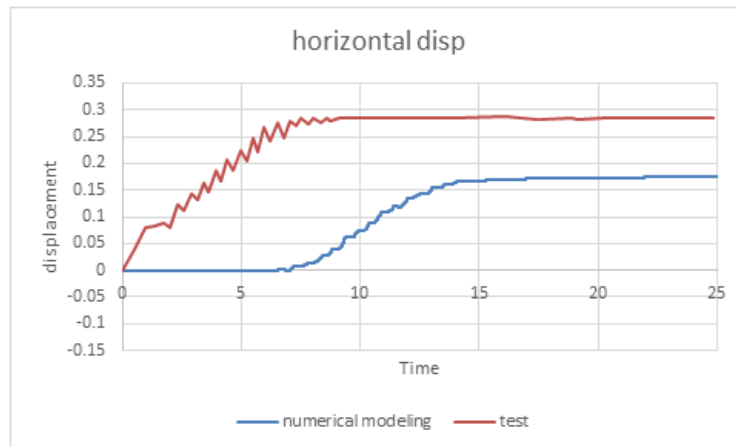


Figure 9. Horizontal displacement of wall after earthquake

It is observed that the process of lateral displacement of the wall is relatively compatible with the results of VELACS11 centrifuge test, but the values of numerical modeling are lower than those recorded for the test. The differences in numerical and experimental modelings may be due to the parameters applied in the Manzari-Dafalias

model to predict the behavior of saturated sand and the impossibility of accurate modeling of pier structure in contact with the soil. Figure 10 demonstrates the liquefaction-induced permanent horizontal displacement of the wall using numerical modeling.

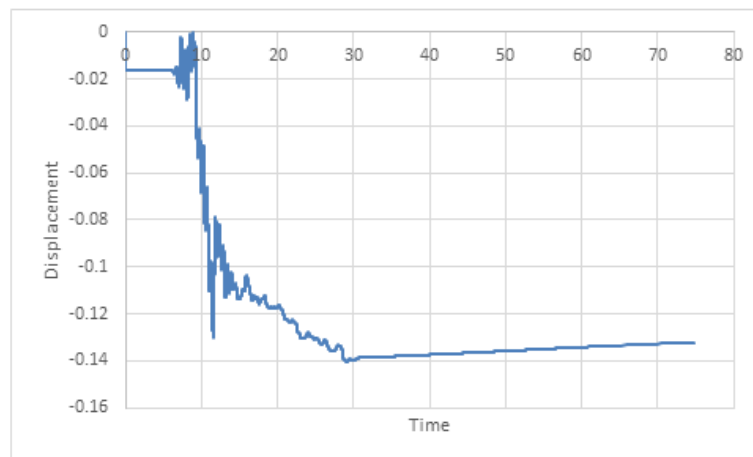
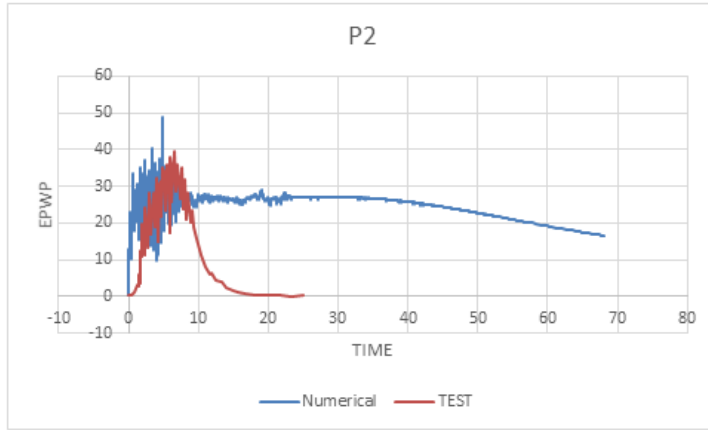


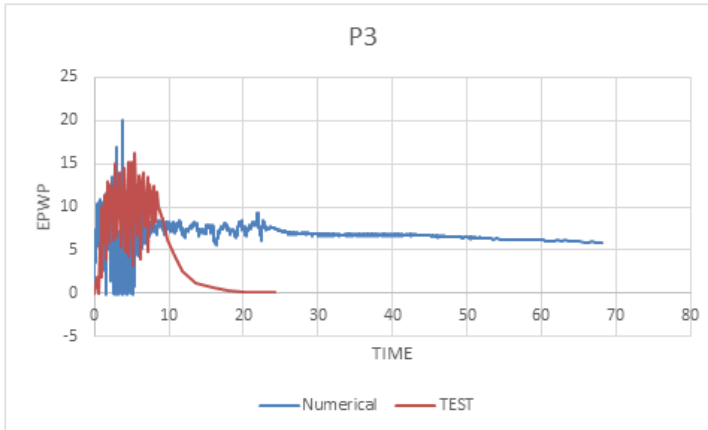
Figure 10. Liquefaction-induced vertical displacement of wall

Given the lack of results of physical modeling, it is not possible to compare the results directly. However, the figure reveals a 14 cm liquefaction-induced settlement in the backfill, which may cause serious damage to the backfill structures. Figure 11 shows the excess pore water pressures

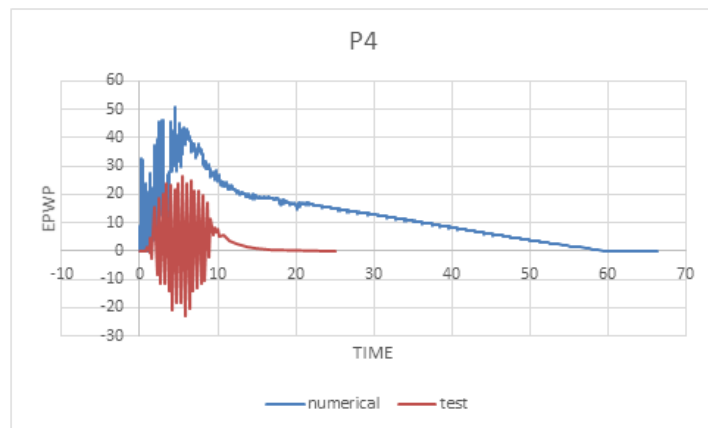
during the test at Cambridge University and the values predicted by numerical modeling using the Manzari-Dafalias model.



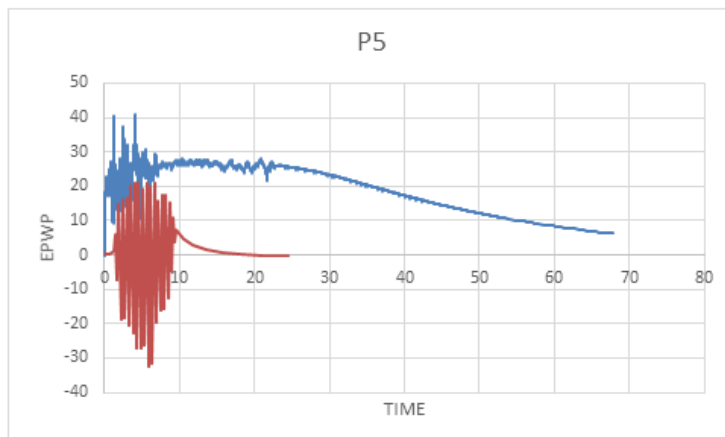
(a)



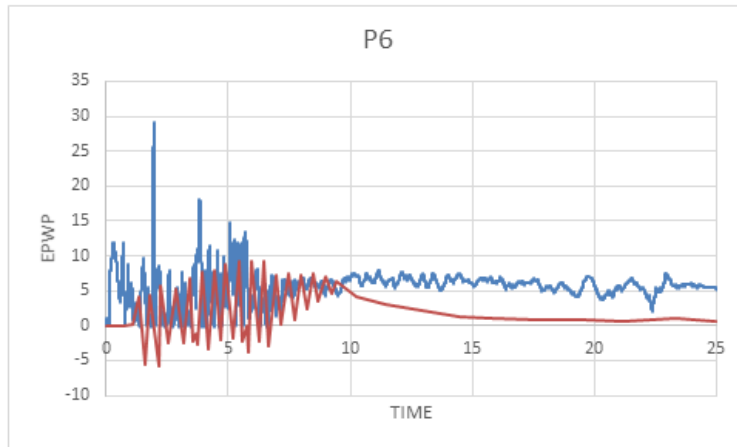
(b)



(c)



(d)



(e)

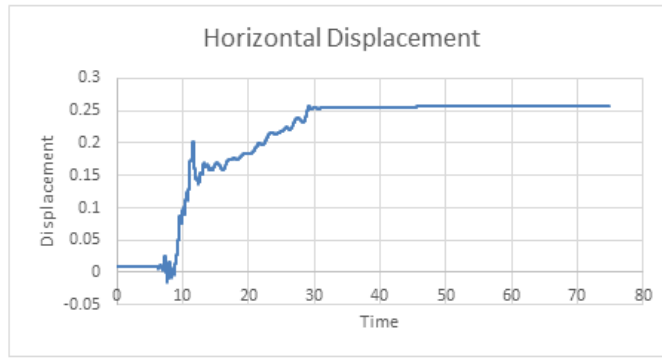
Figure 11. Variations of excess pore water pressure

Figure 11a,b,c,d,e shows the variations of excess pore water pressure at pressuremeters P2, P3, P4, P5 and P6. Given the pressuremeter results, there is good agreement between the increasing trend of pore water pressure in the modeling and the test results. There is a slight difference between the predicted maximum pore water pressure and the test results, which may be due to the incapability of methods used for the accurate modeling of behavior of liquefied sand under low effective stresses and similar rules in centrifuge tests. The difference in dissipation of pore water pressure may also be due to the water used in the tests and variation of permeability versus draining velocity of water. Moreover, there is relatively good agreement between the test results and the numerical modelings of development process of pore water pressure when the input acceleration and predicted maximum pressure are applied. Given the variation of excess pore water pressure at P4, although the numerical model can predict the fluctuation of pore water pressure

between positive and negative values and, in fact, the suction created in the backfill, it succeeds in the prediction of maximum pore water pressure and its variation. The variations of excess pore water pressure at P5 indicate that the numerical model cannot predict the fluctuation of pore water pressure and suction created in the backfill. This may be due to the incapability of formulation used for the accurate modeling of behavior of sand and prediction of suction state and the impossibility of accurate modeling of behavior of pier structure. There is relatively good agreement between the predicted maximum pore water pressure and the test results and they just have a difference of about 20%. This is also observed in the pore water pressure at P6, which may be due to the incapability of model to predict the complicated soil behavior simultaneously affected by wall displacement and impermeability, displacement of liquefied soil and weight and impermeability of lead plate, considering the position of this pressuremeter.



(a)

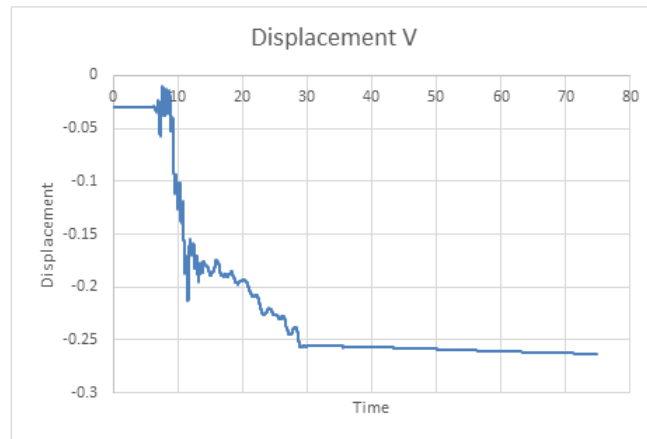


(b)

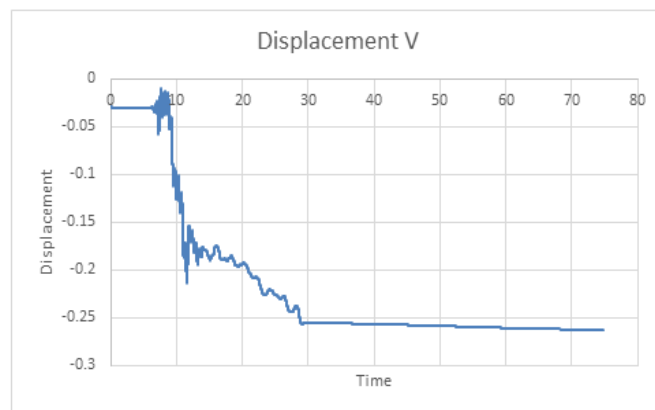
Figure 12. Horizontal displacement of wall: (a) 7 in height; (b) 8 m in height

Figure 12a,b indicates the horizontal displacement of walls 7 and 8 m in height, respectively; so that there are horizontal displacements of 25 cm and 28 cm in the crest of walls 7 m and 8 m in height, respectively, which may cause intensive failures in the structures embedded in the backfill, e.g. pipelines, and surrounding areas. Figure 13a,b represents the vertical displacement of walls 7 and 8 m in height,

respectively. Figure 13a shows a settlement by 26 cm in the backfill. The settlement may cause serious damage to adjacent structures. According to Figure 13b, it is found that the vertical displacement at the top of the wall 8 m high is almost 43 cm. The settlement in the backfill can also cause failure of adjacent structures and heavy damage.



(a)

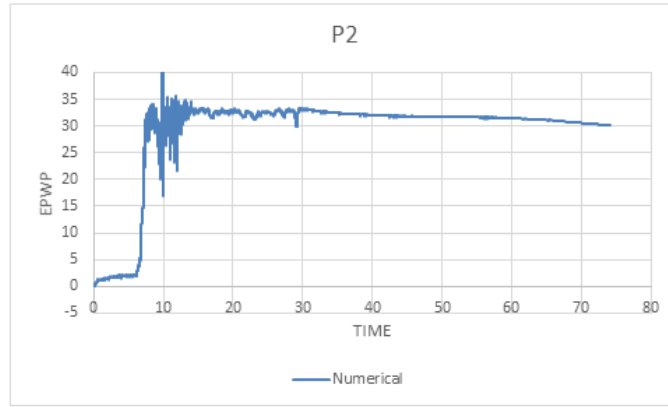


(b)

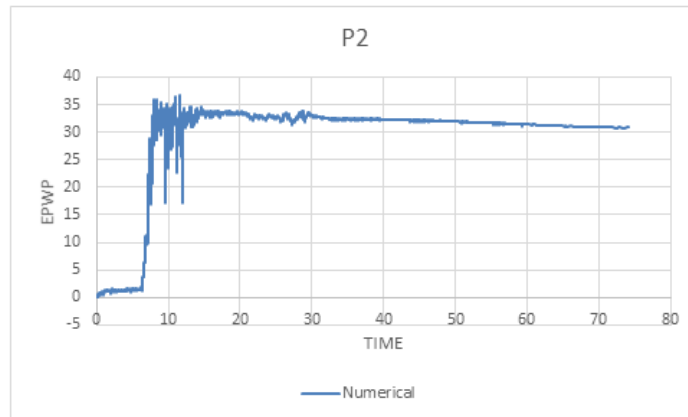
Figure 13. Vertical displacement of wall: (a) 7 in height; (b) 8 m in height

For the wall 7 m high, a comparison of excess pore water pressure at a depth of 1 m in two states of with/without distance from the wall suggests that the earthquake-induced excess pore water pressure does not depend on the

distance of the node from the wall at low depths and the development and dissipation processes of excess pore water pressure are similar (Figure 14).



(a)

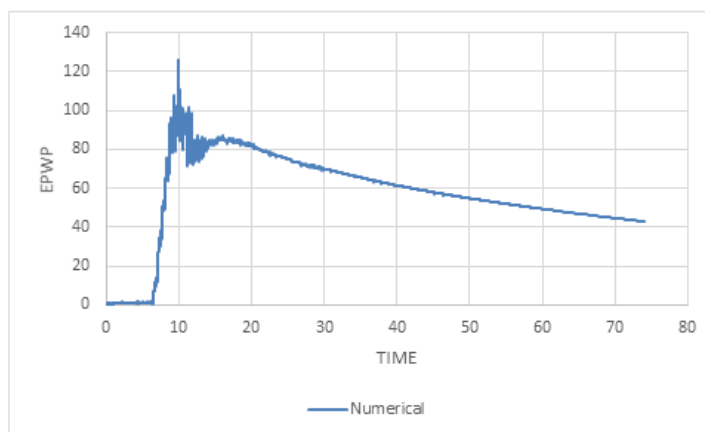


(b)

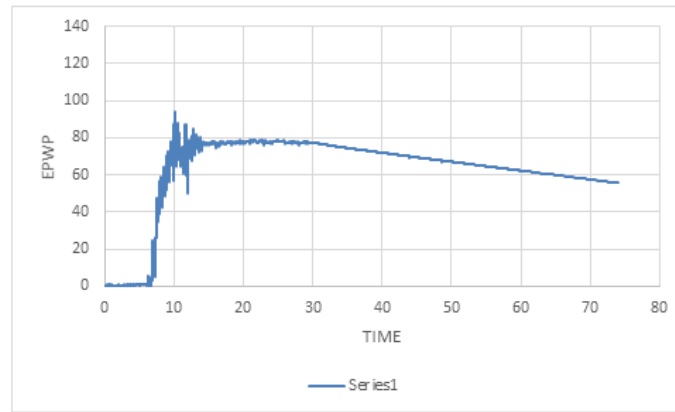
Figure 14. Excess pore water pressure at depth of 1 m for wall 7 m in height: (a) without distance from back of wall; (b) with distance from back of wall

Similar to the wall 7 m in height, the wall 8 m high also has a minor effect on excess pore water pressure at low depths. Figure 15 shows the excess pore water pressure at a depth of 7 m in two states of with/without distance from the wall 7 m in height. According to the figure, it is found

that as the distance from the wall rises at high depths, its effect increases. Therefore, as the distance from the wall increases, the excess pore water pressure decreases in the back of the wall.



(a)



(b)

Figure 15. Excess pore water pressure at depth of 7 m for wall 7 m in height: (a) without distance from back of wall; (b) with distance from back of wall

Assessing the excess pore water pressure for the wall 8 m in height, it is found that the maximum effect of the wall on excess pore water pressure occurs at a depth of 4 m, while this effect is far less at a depth of 8 m, i.e. the bottom of the wall.

4. CONCLUSION

In this study, the impact of liquefaction and lateral spreading on coastal structures is evaluated using numerical methods via OpenSees finite element software. In the numerical model, soil mass is modeled as a continuous medium in accordance with the interaction of solid and fluid phases by correlation and the u-P correlated formulation governing saturated porous media is applied. For more accurate modeling of seismic behavior of saturated sand, the concept of variable permeability is employed during liquefaction in order to estimate the settlement and lateral displacement and predict the rate of development and dissipation of pore water pressure with less error. The results of this study are presented as follows:

1. The modeling properly indicates the vulnerability of piers and gravity quay structures to earthquakes and reveals the importance of revisions to the design codes and standards of these significant structures with the aim of reduction of failures.
2. In the numerical modeling of VELACS11 test, the liquefaction-induced lateral displacement of the wall is relatively compatible with the results of VELACS11 centrifuge tests. The differences in numerical and experimental modelings may be due to the parameters of Manzari-Dafalias model used for the sand and the impossibility of accurate modeling of pier structure.
3. In the numerical modeling of VELACS11, the results of centrifuge tests are suitably compatible with the increasing trend of pore water pressure when the input acceleration is applied and the dissipation of pore water pressure when the acceleration reaches zero. The differences in numerical and experimental modelings of changes in pore

water pressure can be due to the incapability of methods used for accurate modeling of behavior of liquefied sand under low effective stresses, impossibility of accurate modeling of pier structure in VELACS11 test, boundary conditions of the test box and similar rules in centrifuge tests. Given the effect of velocity and wall displacement on pore water pressure created in the backfill, the error in modeling of wall lateral displacement can increase the error in prediction of pore water pressure.

4. Given the horizontal displacement during static analysis, the suction occurs in the backfill, which causes fluctuations in the pore water pressure.
5. The selected time step have a significant influence on the satisfaction of stability condition, accuracy of equilibrium and flow equations and reliability of results; so the time step of $\Delta t = 0.002 \text{ sec}$ is applied in the modeling of VELACS11 test. In each modeling, it is necessary to determine appropriate time step through sensitivity analysis or other existing methods in order to satisfy stability condition and accuracy of calculations and keep the analysis calculations and time at a reasonable level.
6. As the distance from the back of retaining wall increases, the excess pore water pressure declines at a specific depth. This is more considerable at middle parts of the retaining wall.

FUNDING/SUPPORT

Not mentioned any Funding/Support by authors.

ACKNOWLEDGMENT

Not mentioned any acknowledgment by authors.

AUTHORS CONTRIBUTION

This work was carried out in collaboration among all authors.

CONFLICT OF INTEREST

The author (s) declared no potential conflicts of interests with respect to the authorship and/or publication of this paper.

REFERENCES

- Kramer SL. Performance-based design methodologies for geotechnical earthquake engineering. *Bulletin of Earthquake Engineering*. 2014;12(3):1049-70.
- Baska DA. An analytical/empirical model for prediction of lateral spread displacements. 2003.
- Naseri F, Iotfollahi S, Bagherzadeh khalkhali A. Dynamic Mechanical Behavior of Rock Materials. *Journal of Civil Engineering and Materials Application*. 2017;1(2):39-44.
- Youd TL, Perkins DM. Mapping of liquefaction severity index. *Journal of Geotechnical Engineering*. 1987;113(11):1374-92.
- Ghalandarzadeh A, Orita T, Towhata I, Yun F. Shaking table tests on seismic deformation of gravity quay walls. *Soils and foundations*. 1998;38(Special):115-32.
- Taboada V, Abdoun T, Dobry R, editors. Prediction of liquefaction-induced lateral spreading by dilatant sliding block model calibrated by centrifuge tests. *Proc, 11th World Conf on Earthquake Engineering*; 1996: Pergamon Oxford, UK.
- Gonzalez L, Abdoun T, Sharp MK. Modelling of seismically induced liquefaction under high confining stress. *International Journal of Physical Modelling in Geotechnics*. 2002;2(3):01-15.
- Tamate S, Towhata I. Numerical simulation of ground flow caused by seismic liquefaction. *Soil Dynamics and Earthquake Engineering*. 1999;18(7):473-85.
- Hadush S, Yashima A, Uzuoka R. Importance of viscous fluid characteristics in liquefaction induced lateral spreading analysis. *Computers and Geotechnics*. 2000;27(3):199-224.
- Byrne PM. A model for predicting liquefaction induced displacement. 1991.
- Sáez E, Ledezma C. Liquefaction mitigation using secant piles wall under a large water tank. *Soil Dynamics and Earthquake Engineering*. 2015;79:415-28.
- Boulanger RW, Khosravi M, Khosravi A, Wilson DW. Remediation of liquefaction effects for an embankment using soil-cement walls: Centrifuge and numerical modeling. *Soil Dynamics and Earthquake Engineering*. 2018;114:38-50.
- Dewoolkar M, Ko H-Y, Pak R. Experimental developments for studying static and seismic behavior of retaining walls with liquefiable backfills. *Soil Dynamics and Earthquake Engineering*. 2000;19(8):583-93.
- Hung W-Y, Lee C-J, Hu L-M. Study of the effects of container boundary and slope on soil liquefaction by centrifuge modeling. *Soil Dynamics and Earthquake Engineering*. 2018;113:682-97.
- Liu H, Song E. Working mechanism of cutoff walls in reducing uplift of large underground structures induced by soil liquefaction. *Computers and Geotechnics*. 2006;33(4-5):209-21.
- Liu C, Tang L, Ling X, Deng L, Su L, Zhang X. Investigation of liquefaction-induced lateral load on pile group behind quay wall. *Soil Dynamics and Earthquake Engineering*. 2017;102:56-64.
- Tang L, Ling X, Zhang X, Su L, Liu C, Li H. Response of a RC pile behind quay wall to liquefaction-induced lateral spreading: a shake-table investigation. *Soil Dynamics and Earthquake Engineering*. 2015;76:69-79.
- Alyami M, Rouainia M, Wilkinson S. Numerical analysis of deformation behaviour of quay walls under earthquake loading. *Soil Dynamics and Earthquake Engineering*. 2009;29(3):525-36.
- Zienkiewicz OC, Chan A, Pastor M, Schrefler B, Shiomi T. *Computational geomechanics*: Citeseer; 1999.
- Taiebat M, Shahir H, Pak A. Study of pore pressure variation during liquefaction using two constitutive models for sand. *Soil Dynamics and Earthquake Engineering*. 2007;27(1):60-72.
- Dafalias YF, Manzari MT. Simple plasticity sand model accounting for fabric change effects. *Journal of Engineering mechanics*. 2004;130(6):622-34.
- Biot MA. Theory of propagation of elastic waves in a fluid-saturated porous solid. II. Higher frequency range. *The Journal of the acoustical Society of America*. 1956;28(2):179-91.
- Li X-S, Wang Y. Linear representation of steady-state line for sand. *Journal of geotechnical and geoenvironmental engineering*. 1998;124(12):1215-7.
- Ishihara K, Tatsuoka F, Yasuda S. Undrained deformation and liquefaction of sand under cyclic stresses. *Soils and foundations*. 1975;15(1):29-44.
- Newmark NM. Effects of earthquakes on dams and embankments. *Geotechnique*. 1965;15(2):139-60.
- Newmark NM. A method of computation for structural dynamics. *ASCE J Eng Mech div*. 1959;85:67.
- Das BM, Sobhan K. *Principles of geotechnical engineering*: Cengage learning; 2013.
- Helal AA. *Axially loaded pile behavior in sands with/without limited liquefaction*: The University of Alabama in Huntsville; 2012.
- OpenSees MF. *Open system for earthquake engineering simulation*. Pacific Earthquake Engineering Research Center, University of California ...; 2013.
- Maharjan M, Takahashi A. Centrifuge model tests on liquefaction-induced settlement and pore water migration in non-homogeneous soil deposits. *Soil Dynamics and Earthquake Engineering*. 2013;55:161-9.
- Shahir H, Pak A, Taiebat M, Jeremić B. Evaluation of variation of permeability in liquefiable soil under earthquake loading. *Computers and Geotechnics*. 2012;40:74-88.